

Thermoelectric transport properties of gapless pinned charge density waves

Tomas Andrade¹ and Alexander Krikun²

¹*Departament de Física Quàntica i Astrofísica, Institut de Ciències del Cosmos, Universitat de Barcelona, Martí i Franquès 1, E-08028 Barcelona, Spain*

²*Nordita, KTH Royal Institute of Technology and Stockholm University
Hannes Alfvénsgatan 12, SE-106 91 Stockholm, Sweden*

Quantum strongly correlated matter exhibits properties which are not easily explainable in the conventional framework of Fermi liquids. Universal effective field theory tools are applicable in these cases regardless of the microscopic details of the quantum system, since they are based on symmetries. It is necessary, however, to construct these effective tools in full generality, avoiding restrictions coming from particular microscopic descriptions which may inadequately constrain the coefficients that enter in the effective theory.

In this work we demonstrate on explicit examples how the novel hydrodynamic coefficients which have been recently reinstated in the effective theory of pinned charge density waves (CDW) can affect the phenomenology of the thermo-electric transport in strongly correlated quantum matter. Our examples, based on two classes of holographic models with pinned CDW, have microscopics which are conceptually different from Fermi liquids. Therefore, the above novel transport coefficients are nonzero, contrary to the conventional approach. We show how these coefficients allow to take into account the change of sign of the Seebeck coefficient and the low resistivity of the CDW phase of the cuprate high temperature superconductors, without referring to the effects of Fermi surface reconstruction.

I. INTRODUCTION

The transport properties of the charge density wave (CDW) ordered states of strongly entangled quantum matter, and in particular in cuprate superconductors, have attracted a great deal of attention over the years. The CDW plays an important role in the phase diagram of the cuprates: it appears as an order parameter in a subregion across the pseudogap and superconductor phases, as well as a fluctuation at higher temperatures in the strange metal phase¹. It can be demonstrated quite clearly² that the onset of CDW leaves an imprint on the thermopower (or Seebeck coefficient), which starts decreasing at the CDW critical temperature T_{CDW} and reaches negative values at low T 's. This feature is observed in a variety of different compounds^{3–8} and can be considered as a universal signature of CDW. From the point of view of the Fermi liquid theory, this behavior may be understood as a reconstruction of the Fermi surface⁹ (to date, yet to be detected). However, the very applicability of the Fermi liquid to cuprates is debatable^{10–12} and the need to alternative approaches to the physics of thermopower in these systems persists^{13,14}.

Irrespective of the microscopic description of a particular physical system, one can construct an effective theory description (EFT) of its low energy properties by making use of symmetry considerations¹⁵. In the case of exact global symmetries, these procedure leads to hydrodynamics¹⁶. If a certain global symmetry is spontaneously broken, the corresponding Goldstone mode appears in the spectrum and must be added to the hydrodynamic degrees of freedom. In this way, one constructs e.g. superfluid hydrodynamics^{17,18}. In cases in which the spontaneously broken symmetry is only approximate (there is a small explicit symmetry breaking source), the

massive pseudo-Goldstone mode can be included in the hydrodynamic description^{19–22}. The phases of matter with pinned CDW fall in this latter class: the spatial structure of CDW breaks translation symmetry spontaneously, while pinning provides an explicit symmetry breaking source.

The effective theory of broken translations has long been appreciated as a tool to address the dynamics of the CDW phases in quantum systems²³. Recently, it has experienced a renaissance motivated in part by the appearance of a novel class of physical models described by the holographic duality^{24,25}. These models, on one hand, exhibit the weakly pinned CDW phases^{26–28} (see²⁹ for recent review) and therefore must be describable by a symmetry based EFT. On the other hand, they completely defy the principles of gapped Fermi liquid, which were used in the earlier EFT constructions to constrain certain hydrodynamic coefficients. Therefore, the need to relax some of these constraints has been identified recently and this has led to a new generation of effective theories of pinned CDW, with an enlarged set of nonzero hydrodynamic coefficients^{19–21,30,31}.

In this work we study explicit examples of translational symmetry breaking phases in holographic models. We evaluate the full set of AC and DC thermo-electric conductivities and match the results with the EFT description of^{19,20,31}. We show that the novel transport coefficients, namely, the incoherent conductivity and Goldstone mode diffusivity, are finite in the considered examples and lead in turn to the novel phenomenology: the change of sign of the Seebeck coefficient discussed above, and the weak resistivity of the symmetry broken state. The latter is another puzzling phenomenon observed in CDW phase of cuprates^{32–34}.

In the following Section we review the hydrodynamic

effective theory of pinned CDWs. Then, we construct the holographic dual to a quantum system with CDW order and show that its AC conductivity, as expected, is described perfectly well with the EFT, however with the parameters which do not follow the conventional Fermi liquid logic. We obtain the DC conductivities and demonstrate the novel phenomenological features, which may be observed experimentally. In the Supplementary material we present the details of the two holographic models which we studied, the set of checks which we perform on the AC spectra as well as some additional results in a different holographic model based on helical Bianchi VII geometries.

II. EFFECTIVE THEORY OF CHARGE DENSITY WAVES

A usual consequence of spontaneous symmetry breaking is the appearance of a massless degree of freedom in the spectrum – the Goldstone boson. In case of CDW, the Goldstone boson – or sliding mode – is simply a shift of the whole spontaneously formed structure along the broken direction in space.

In a hydrodynamic approach, the effective theory of pinned CDW can be built in a way completely analogous to superfluid hydrodynamics^{20–22,30,31,35}. Importantly, the effective hydrodynamic approach based on symmetries is valid irrespective of whether the quantum system admits a perturbative treatment or not. Thus, it forms a convenient basis for the analysis of various experimental measurements, allowing one to express large volumes of data in terms of a limited number of hydrodynamic coefficients, which are the free parameters of the model.

We will now summarize the necessary results of the effective theory description of CDW developed in^{30,31,36}. For the sake of brevity, let us immediately restrict the general model of³¹ to a space-time with 2 spacial dimensions (x, y)-³⁷ with an unidirectional spontaneous spatial structure, which is the CDW. Introducing an intrinsic coordinate ϕ along the only modulation direction of the CDW, one can characterize its embedding in space by a single “crystal field” $\phi(x, y)$. The ground state is a homogeneous CDW with no defects, modulated along the x -axis, and corresponds simply to $\phi_0(x, y) = \alpha x$.³⁸ Note that the translation of the CDW as a whole – the sliding mode – is encoded in the shifts of ϕ : $\phi \rightarrow \phi + \delta\phi$ and is equivalent to translating the CDW along the x -axis by $\delta x = \delta\phi/\alpha$. Therefore one readily identifies ϕ as a Goldstone field.

We further restrict our attention to small low-frequency, long-wavelength fluctuations of the CDW structure along the x -direction only: $\phi = \phi_0 + \alpha\delta\phi(t, x)$. Similarly, we introduce fluctuations in the local chemical potential $\mu = \mu_0 + \delta\mu(t, x)$ and temperature $T = T_0 + \delta T(t, x)$, as well as in the local velocity field $u_\mu = \{1, 0, 0\} + \delta u_\mu(t, x)$. For the purpose of computing the two-point functions relevant for transport properties, we

consider external sources for the current and energy-momentum tensor: the electric field $\delta\partial_t A_x(t, x)$ and the background metric perturbation $\delta g_{tx}(t, x)$. Moreover, we take into account the effect of the crystal lattice, which simultaneously breaks translations explicitly, introducing a finite momentum dissipation Γ , and pins the CDW, providing a mass m_ϕ^2 to the Goldstone mode. As long as Γ and m_ϕ^2 can be considered to be small, this “weak pinning” effect can be treated as a small correction to the hydrodynamic conservation laws. Finally, as it has been studied in detail in^{19–22,35,36,39}, the pinning leads to a finite lifetime of the Goldstone, parametrized by the phase relaxation term Ω . The full set of hydrodynamic constitutive relations, resulting from the framework of^{19,20,31} in this case is listed in the Supplementary Material (A1). The expressions for the electric current and the Goldstone configuration equation (Josephson relation) including the relaxation term are particularly relevant for our discussion⁴⁰

$$J^x = \rho\delta u_x + \gamma(\partial_t\delta\phi - \delta u_x) - \sigma_q \left(T_0\partial_x \frac{\mu}{T} + \partial_t\delta A_x \right), \quad (1)$$

$$\begin{aligned} \partial_t\delta\phi - \delta u_x - \frac{B+G}{\sigma_\phi}\partial_x^2\delta\phi \\ - \frac{\gamma'}{\sigma_\phi} \left(T_0\partial_x \frac{\mu}{T} + \partial_t\delta A_x \right) = -\Omega\delta\phi. \end{aligned} \quad (2)$$

In addition, we quote the stress-energy and current conservation laws, modified by the explicit sources and symmetry breaking terms

$$D_\mu T_t^\mu = 0, \quad D_\mu J^\mu = 0 \quad (3)$$

$$D_\mu T_x^\mu = -\rho\partial_t\delta A_x + \Gamma T_{tx} - Gm_\phi^2\delta\phi \quad (4)$$

Here $\{P, \rho, s\}$ are thermodynamic pressure, charge density and entropy in the ground state, $\{B, G\}$ are bulk and shear elastic moduli of the spontaneous structure, $\{\zeta, \eta\}$ are bulk and shear viscosities, while $\{\sigma_q, \gamma, \gamma', \sigma_\phi\}$ are 4 more hydrodynamic coefficients which we discuss now in more detail.

The σ_q and σ_ϕ^{-1} coefficients are usually set to zero in the standard treatment of CDW in gapped quantum systems²³. If we examine the Josephson relation in absence of perturbative sources and pinning, we see that at any finite momentum k the Goldstone mode decays with the rate $\sigma_\phi^{-1}(B+G)k^2$, therefore σ_ϕ^{-1} controls the Goldstone diffusivity^{27,41}. However in the quantum system with a gap, the Goldstone mode cannot decay even at finite momentum, unless the momentum is large enough to cross the gap. Therefore, at zero temperature one sets $\sigma_\phi^{-1} = 0$ and all terms except δu_x drop out from (2). On the other hand, at finite temperature one expects σ_ϕ^{-1} to be exponentially suppressed by the scale of the gap.

The other unusual coefficient is σ_q . This piece is allowed from the EFT perspective, but it is absent in systems where transport is mediated by quasiparticles and the current is constrained by Galilean symmetry $J^x = \rho\delta u^x$. This coefficient is related to “incoherent con-

ductivity" which has been discussed extensively in connection to holographic models^{42–45} and plays a crucial role here.

We can plug in the constitutive relations into the conservation laws and solve the system of differential equations with respect to hydrodynamic variables $\{\delta u_x, \delta \mu, \delta T, \delta \phi\}$ in presence of external sources $\{\delta A_x, \delta g_{tx}\}$. Inserting the solutions back into the constitutive relations, we obtain the expectation values for various operators in terms of perturbative sources¹⁶. This allows us to evaluate the two point functions $\langle J^x J^x \rangle$, $\langle J^x T^{tx} \rangle$, $\langle T^{tx} J^x \rangle$, and $\langle T^{tx} T^{tx} \rangle$. As one can show from locality of the hydrodynamic equations¹⁹, positivity of entropy production²⁰, or the Onsager relation between $\langle J^x T^{tx} \rangle$ and $\langle T^{tx} J^x \rangle$ (see Supplementary material II) the coefficients are related as^{27,35,36,41,46–50}.

$$\gamma' = -\gamma, \quad \Omega = \sigma_\phi^{-1} m_\phi^2 G. \quad (5)$$

Recalling the definition of the heat current in presence of a finite chemical potential⁵¹: $Q^x = J^x + \mu T^{tx}$, we arrive at the full matrix of AC thermoelectric conductivities⁵²

$$\begin{pmatrix} J^x \\ Q^x \end{pmatrix} = \begin{pmatrix} \sigma & T\alpha \\ T\bar{\alpha} & T\bar{\kappa} \end{pmatrix} \begin{pmatrix} E_x \\ -\frac{\partial_x T}{T} \end{pmatrix} \quad (6)$$

at zero wavelength limit:

$$\begin{aligned} \sigma(\omega) &= \sigma_0 + \frac{\tilde{\rho}^2(\Omega - i\omega) - \tilde{\gamma}^2\omega_0^2(\Gamma - i\omega) - 2\tilde{\rho}\tilde{\gamma}\omega_0^2}{\mu_0^2\chi_{\pi\pi}((\Gamma - i\omega)(\Omega - i\omega) + \omega_0^2)} \\ \frac{T}{\mu_0}\alpha(\omega) &= -\sigma_0 + \frac{\tilde{\rho}\tilde{s}(\Omega - i\omega) + \tilde{\gamma}^2\omega_0^2(\Gamma - i\omega) - (\tilde{s} - \tilde{\rho})\tilde{\gamma}\omega_0^2}{\mu_0^2\chi_{\pi\pi}((\Gamma - i\omega)(\Omega - i\omega) + \omega_0^2)} \\ \frac{T}{\mu_0^2}\bar{\kappa}(\omega) &= \sigma_0 + \frac{\tilde{s}^2(\Omega - i\omega) - \tilde{\gamma}^2\omega_0^2(\Gamma - i\omega) + 2\tilde{s}\tilde{\gamma}\omega_0^2}{\mu_0^2\chi_{\pi\pi}((\Gamma - i\omega)(\Omega - i\omega) + \omega_0^2)}, \end{aligned} \quad (7)$$

where

$$\begin{aligned} \sigma_0 &= \sigma_q + \frac{\gamma^2}{\sigma_\phi}, \quad \tilde{\rho} = \mu_0\rho, \quad \tilde{s} = T_0s, \quad \chi_{\pi\pi} = \tilde{\rho} + \tilde{s} \quad (8) \\ \tilde{\gamma} &= \mu_0\chi_{\pi\pi}\gamma/\sigma_\phi, \quad \omega_0^2 = Gm_\phi^2/\chi_{\pi\pi}. \end{aligned}$$

In the ordered state far from T_c these expressions correspond to the peak in the real part of the spectra, located at finite "pinning frequency" ω_0 with width $(\Omega + \Gamma)$. This is a manifestation of the gapped coherent sliding mode. The DC conductivities display a mixture of coherent and incoherent contributions, which can be recast as

$$\begin{aligned} \sigma &= \sigma_q + \sigma_\phi^{-1} \frac{(\rho - \gamma)^2}{1 + \frac{\Gamma\chi_{\pi\pi}}{\sigma_\phi}}, \quad \frac{\bar{\kappa}T}{\mu^2} = \sigma_q + \sigma_\phi^{-1} \frac{(\frac{sT}{\mu} + \gamma)^2}{1 + \frac{\Gamma\chi_{\pi\pi}}{\sigma_\phi}}, \\ \frac{\alpha T}{\mu} &= -\sigma_q + \sigma_\phi^{-1} \frac{(\rho - \gamma)(\frac{sT}{\mu} + \gamma)}{1 + \frac{\Gamma\chi_{\pi\pi}}{\sigma_\phi}}. \end{aligned} \quad (9)$$

These expressions represent the main outcome of the EFT^{19,30,35}, which we are going to study. Note that both terms are usually negligible in the conventional gapped

CDW: σ_q is zero because of Galilean invariance, while σ_ϕ^{-1} is exponentially suppressed due to a gap in the quantum spectrum. This leads to a hard insulating behavior of the conventional pinned CDW.

In presence of finite σ_q and σ_ϕ^{-1} , however, the DC conductivities depart from the conventional picture. Firstly, the electric conductivity is finite even in the broken phase, and secondly, the sign of the thermopower α is a result of the interplay between σ_q and σ_ϕ^{-1} terms. In what follows we explore how this novel mechanisms come about in non-Fermi liquid, holographic models.

III. HOLOGRAPHIC MODEL OF GAPLESS CDW

The essence of holographic modelling is the correspondence between strongly entangled quantum systems and classical black holes in auxiliary spacetimes, which are constructed according to a rigorous set of rules – the "holographic dictionary"^{24,25,51,52}. In this paradigm, the quantum system at finite temperature T and chemical potential μ in a 2+1 dimensional space-time corresponds to a black hole in a 3+1 dimensional curved space-time, whose horizon radius and charge are set by T and μ . The crystal lattice can be introduced via periodic modulation of the chemical potential^{53–59}: $\mu(x) = \mu_0(1 + A \cos(kx))$ ⁶⁰. We will consider the model with small $A = 0.04$, describing the weakly pinned CDW. The spontaneous structure formation is realized as an instability of the black hole against formation of the spatially modulated "hair"^{61–63}: as the temperature gets lowered certain fields condense outside the black hole horizon. The interplay between the explicit and spontaneous translation symmetry breaking has been studied extensively in this setup^{39,64–66}, note also other approaches⁶⁷. The action of the model reads

$$S = \int d^4x \sqrt{-g} \left(R - 2\Lambda - \frac{1}{2}(\partial\psi)^2 - \frac{\tau(\psi)}{4}F^2 - W(\psi) \right) - \frac{1}{2} \int \theta(\psi)F \wedge F. \quad (10)$$

where $F = dA$ is the field strength of the $U(1)$ gauge field in a 3+1 dimensional bulk, which is dual to a $U(1)$ global charge symmetry, ψ is an axion field in the bulk coupled to the θ -term, which drives a CDW instability. R and Λ are the Ricci curvature and negative cosmological constant, which govern the structure of asymptotically Anti-de Sitter (AdS) space in the bulk. The qualitative features we reveal depend only mildly on the precise form of the potentials

$$\begin{aligned} \tau(\psi) &= 1 + \dots, & W(\psi) &= -\psi^2 + \dots, \\ \theta(\psi) &= \frac{c_1}{2\sqrt{6}}\psi + \dots, \end{aligned} \quad (11)$$

which we present in more detail in the Methods section.

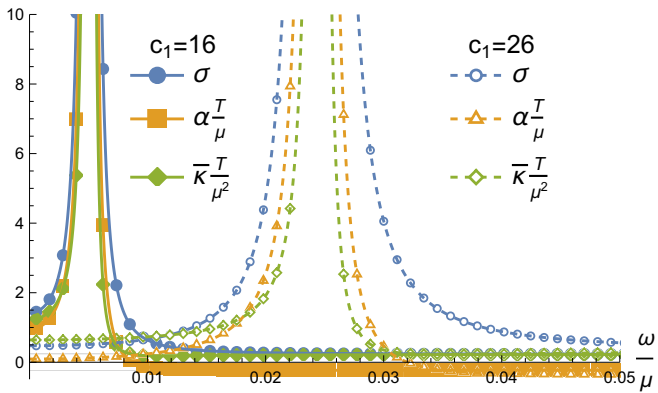


FIG. 1: The pinned peak in AC conductivities. The filled dots and solid lines show the AC data for the conductivities in the holographic model with $c_1 = 16$ and the fits with (7). The empty dots and dashed lines – the same with $c_1 = 26$. Data taken for the 2/1 commensurate states with $T/\mu = 0.1, k/\mu \approx 2.1, A = 0.04$.

The holographic dictionary identifies the asymptotics of the gauge field profile near the AdS boundary (located at radial coordinate $z \rightarrow 0$) with the chemical potential and $U(1)$ charge density: $A_t(x, z) \Big|_{z \rightarrow 0} = \mu(x)z + \rho(x)z^2$. Given the classical solution to the Einstein equations following from (10) with appropriate boundary conditions set by $\mu(x), T$ one can compute the charge density profile $\rho(x)$ and observe formation of spontaneous CDW below a certain critical temperature $T = T_0(c_1)$, which depends on the value of the coupling constant c_1 . The instability is driven by the θ -term in the action. As the temperature is lowered, the order parameter – the amplitude of the charge density modulation – grows and the effective theory of pinned CDW is applicable. One can also achieve the similar growth of the order parameter by tuning the coupling constant c_1 at fixed temperature.

In order to evaluate the AC conductivities, we follow a procedure which is quite similar to the one we used in the previous Section. We introduce the perturbative sources for the electric current and stress-energy tensor, which are now encoded in the near-boundary asymptotes of the bulk gauge field $A_x(z)$ and bulk metric $g_{tx}(z)$. After solving the equations of motion in the bulk, we read off the subleading profile components in these fields, which give us the expectation values of the dual operators $\langle J^x \rangle$ and $\langle T^{tx} \rangle$. In this way we obtain the 2-point functions $\langle J^x J^x \rangle$, $\langle J^x T^{tx} \rangle$, $\langle T^{tx} J^x \rangle$, and $\langle T^{tx} T^{tx} \rangle$ and therefore the matrix of AC thermoelectric conductivities (6). The corresponding numerical calculations are quite demanding, especially at low temperatures. Therefore when studying the phenomenology of the AC transport we fix the temperature and tune the coupling constant in order to control the order parameter. We present the technical details in the Supplementary material B.

In the weak pinning regime ($A = 0.04$), the results have precisely the shape predicted by the effective theory, see Fig.1: the peak located at finite frequency ω_0 . As we discuss in more detail in the Supplementary material C, given these AC line-shapes we can perform a set of cross-checks of the model expressions (1). Firstly, we obtain the same values of hydrodynamic coefficients when independently fitting σ, α and κ . Moreover, we can extract thermodynamic data from the AC linear response fits, which agree with the data obtained as the operator expectation values in the ground state of the model. This check also shows that the extra thermodynamic quantities, discussed in^{20,30}, like the lattice pressure, play at most a subleading role in our treatment and can be safely neglected. Finally, we get excellent agreement between the DC conductivities, obtained by the expressions (9) using the values of the hydrodynamic coefficients from the AC fits, and the DC transport properties evaluated using the near horizon data in the holographic ground state, as we discuss in a moment. All these checks support the statement that the effective theory of pinned CDW, outlined in Sec. II does indeed describe well the results which we obtain in the holographic model.

IV. DC TRANSPORT

The DC transport features of the holographic model can be studied with much greater precision than the AC conductivities thanks to the method of extracting the DC response from the near horizon geometry of the ground state black hole^{57,68–73}.

The results for temperature series of solutions with different c_1 -coupling are shown on Fig. 2. One can immediately recognize the unconventional behavior of the electric conductivity, which decreases at small temperature as a certain power law, instead of the activated exponential behavior ($\sim \exp(-\Delta_{CDW}/T)$) expected for the gapped CDW state. Moreover the thermopower changes sign at a certain point in temperature, which is dependent of the model coupling c_1 . While being unusual from the point of view of the conventional treatment, this behavior can be well incorporated in the generalized EFT framework of Sec.II. We note also that, as we show on Fig. 3, the DC conductivities are insensitive to the scale of the explicit symmetry breaking (crystal lattice/impurities), as long as it remains small, which supports our treatment of Γ as a small parameter in (9).

In the previous section we established the validity of the EFT description for our holographic model in the regime where the growing order parameter was a result of tuning the coupling constant c_1 at fixed temperature. Assuming that EFT continues to be applicable in the regimes where the order grows due to the decrease of temperature, we can make use of (9) and extract all the hydrodynamic parameters having the DC conductivities at hand (in the weak pinning regime). This calculation leads to the results we show in Fig. 4. We see that the

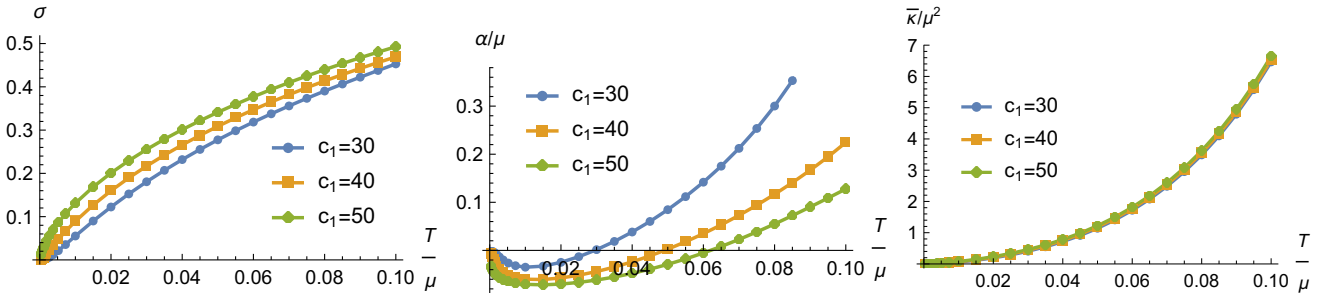


FIG. 2: The evolution DC thermo-electric conductivities at small temperatures. The holographic model with different values of the coupling c_1 is considered. Note that thermopower changes sign at some coupling-dependent point. Data taken for the 2/1 commensurate states with $k/\mu = 2, A = 0.04$.

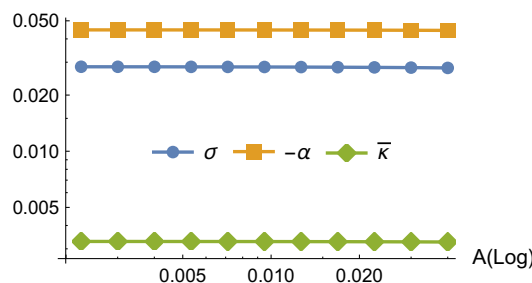


FIG. 3: Dependence of the DC thermo-electric conductivities on the pinning scale A . The data taken for the 2/1 commensurate states with $k/\mu = 2, A = 0.04$

EFT parameters σ_q and σ_ϕ^{-1} , which are responsible for the finite DC values in (9), are indeed non-zero and behave as power laws rather than as gapped exponentials. Note that σ_q is largely insensitive to the coupling constant driving the phase transition, as one would expect it, given that it is not related to the Goldstone mode behavior. The γ -coefficient changes sign at some temperature and saturates at some small fraction of the total charge density ρ .

The relative contributions of the various terms in (9) to the DC transport are shown on Fig. 5. Quite interestingly, we see that the electric conductivity is dominated by the $\sigma_\phi^{-1}\rho^2$ term, while the heat conductivity is rather controlled by σ_q . This means that the behavior of the electric and heat conductivities is not related to each other at the level of EFT. This points out the possible reason why Wiedemann–Franz law may not be satisfied in materials with these “gapless pinned CDW”. Looking at the thermopower, we see that the two terms in (9) are of the same order and cancel each other. This cancellation is the reason of the sign change in α as seen on Fig. 2. It is therefore quite clear that the exact temperature where the sign changes is dependent on the various subleading contributions and therefore does not point to some conceptual change, as it would be the case with the Fermi surface reconstruction.

The phenomenological features which we observe here

are not specific to a particular holographic model. As we show in Supplementary material D, we obtain similar results in a different setup based on a helical lattice. The universal feature, which appears in both cases is the absence of exponential suppression of either σ_q or σ_ϕ^{-1} , leading to a nontrivial interplay between the terms in (9). The remarkable cancellation of terms in α as well as the exchange of dominance of the σ_q and σ_ϕ^{-1} terms in σ and κ are also persistent features in our data. This might point out some universal relation between $\gamma\sigma_\phi^{-1}$ and σ_q as suggested in^{27,41}. There it has been conjectured based on the study of the specific homogeneous holographic model, that at low temperatures γ should saturate the universal relaxation bound $\gamma \sim \frac{\mu}{sT}\sigma_\phi\sigma_0$. However, as we demonstrate in Supplementary material E, we do not observe this particular saturation in our models.

V. CONCLUSION

In this Letter we demonstrate how the novel parameters in the effective theory of pinned charge density waves, discussed in recent constructions^{19–22,30,31,36}, which are absent in gapped quantum systems, affect the thermo-electric transport in cases where they are nonzero. The absence of the clean gap in the spectrum of the quantum model can be a result of the quantum continuum being present in the system, which provides finite spectral density at every energy. The effects of such a continuum spectrum have already been studied earlier in relation to the physics of plasmons⁷⁴, the dynamics of the pattern formation³⁹ and the electron spectral functions^{75–77}.

In the explicit examples constructed by means of holographic duality, we show that the “gapless” pinned charge density waves demonstrate non-vanishing resistivity in the pinned CDW phase, change of sign in the thermopower, unrelated to the reconstruction of the Fermi surface, the conceptual absence of Wiedemann–Franz law in the relation between the thermal and electric conductivities and the low sensitivity of the transport properties to the concentration of the impurities. All these

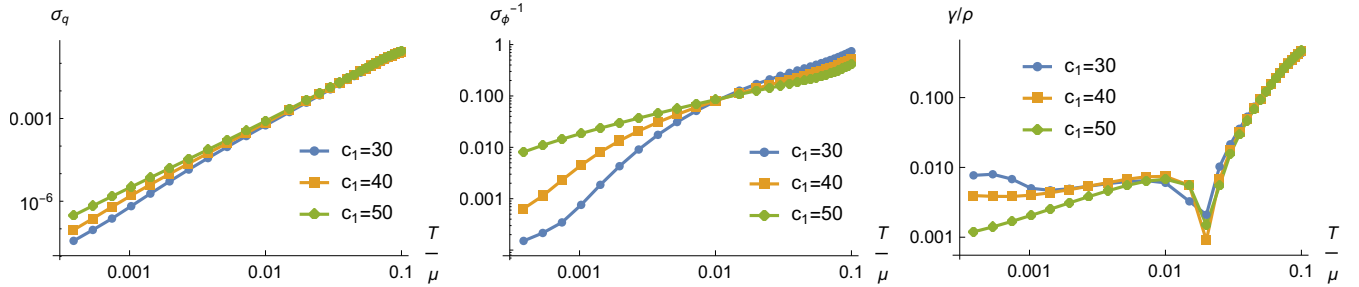


FIG. 4: The behavior of effective theory parameters at low temperatures. Log-Log scales. Incoherent conductivity σ_q and Goldstone diffusivity behave as certain power laws, but the former does not depend on the coupling c_1 . γ changes sign at some $T/\mu \approx 0.02$ for all c_1 . Note that this is not related to the change of sign in α . γ/ρ saturates at some finite value at low T . Same data as on Fig. 3.

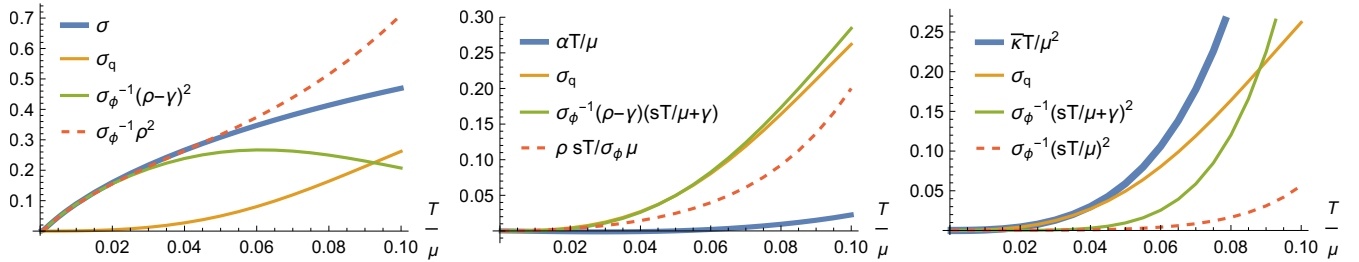


FIG. 5: The contributions to DC conductivities from various terms in (9). At low T electric conductivity is dominated by σ_ϕ^{-1} term, heat conductivity – by σ_q -term, while thermopower is a result of a fine balance between them. Red lines assume $\gamma = 0$ and help to appreciate the role of γ . Data as on Fig. 3 for $c_1 = 40$.

phenomenological features being observed in the under-doped phases of cuprate high temperature superconductors, where charge density waves are present.

We hope that these examples will encourage the use of the improved EFT in the analysis of the transport experiments in CDW cuprates, which in turn could clarify their physical nature and, perhaps, would unveil the properties of the underlying quantum criticality.

We also point out that the phenomenology of the DC transport, described above, being a consequence of the pinned CDW behavior, predicts the specific shapes of the spectra of AC conductivities (7), which makes the experimental on the optical spectroscopy extra important.

It is worth mentioning that when deriving the expressions (9) and (7) and focusing on the qualitative effects, we omitted other novel hydrodynamic coefficients, pointed out in²⁰, which play a subleading role in our discussion. One should keep this in mind when performing precision tests of (9) and (7).

ACKNOWLEDGMENTS

We thank Koenraad Schalm, Jan Zaanen and Floris Balm for long lasting collaboration in this subject. We are grateful to Jay Armas, Akash Jain, Andrea Amoretti, Daniel Brattan and Blaise Gouteraux for useful communication and valuable advice. A.K. thanks Dragana Popovic, Floriana Lombardi, Riccardo Arpaia, Ulf Gran and David Marsh for insightful comments.

A.K. acknowledges the hospitality of the physics department of Chalmers Technical University, where the preliminary results of this work have been discussed.

The work of A.K is supported by VR Starting Grant 2018-04542 of Swedish Research Council. The work of T.A. is supported in part by the ERC Advanced Grant GravBHs-692951 and by Grant CEX2019-000918-M funded by Ministerio de Ciencia e Innovación (MCIN)/Agencia Estatal de Investigación (AEI)/10.13039/501100011033.

The numerical computations were enabled by resources provided by the Swedish National Infrastructure for Computing (SNIC), partially funded by the Swedish Research Council through grant agreement no. 2018-05973, at SNIC Science Cloud and PDC Center for High Performance Computing, KTH Royal Institute of Technology. Nordita is supported in part by Nordforsk.

Appendix A: Effective theory of CDW

In order to derive equations (7) we rely on the framework used in³⁰ and supplement it with the explicit symmetry breaking terms introduced in²¹. We restrict the dynamics to a single x - direction and consider a unidirectional CDW. Neglecting the contributions from lattice pressure and other extra terms considered in^{20,30}, the full set of hydrodynamic constitutive relations reads

$$J^t = \rho + \left(\frac{\partial \rho}{\partial \mu} \delta \mu + \frac{\partial \rho}{\partial T} \delta T \right), \quad (\text{A1})$$

$$J^x = \rho \delta u_x + \gamma (\partial_t \delta \phi - \delta u_x) - \sigma_q \left(T_0 \partial_x \frac{\mu}{T} + \partial_t \delta A_x \right), \quad (\text{A2})$$

$$T^{tt} = \epsilon + \left(\mu_0 \frac{\partial \rho}{\partial \mu} + T_0 \frac{\partial \rho}{\partial T} \right) \delta \mu + \left(\mu_0 \frac{\partial s}{\partial \mu} + T_0 \frac{\partial s}{\partial T} \right) \delta T, \quad (\text{A3})$$

$$T^{tx} = P \delta g_{tx} + (\mu_0 \rho + T_0 s) \delta u_x, \quad (\text{A4})$$

$$T^{xx} = P + \left(s \delta T + \rho \delta \mu + (\zeta + \eta) \partial_x \delta u_x - (B + G) \partial_x \delta \phi - 2\eta \partial_x \delta g_{tx} \right), \quad (\text{A5})$$

$$\partial_t \delta \phi - \delta u_x - \frac{B + G}{\sigma_\phi} \partial_x^2 \delta \phi - \frac{\gamma'}{\sigma_\phi} \left(T_0 \partial_x \frac{\mu}{T} + \partial_t \delta A_x \right) = -\Omega \delta \phi. \quad (\text{A6})$$

Following the procedure outlined in the main text and taking the variations with respect to the sources δg_{tx} , δA_x , we arrive, among others, to the following expressions for the correlation functions

$$\langle J_x T_{tx} \rangle = - \left(\rho(\omega + i\Omega) + i\gamma' \sigma_\phi^{-1} \chi_{\pi\pi} \omega_0^2 \right) / (\omega^2 + i\omega(\Gamma + \Omega) - \Gamma\Omega - \omega_0^2), \quad (\text{A7})$$

$$\langle T_{tx} J_x \rangle = - (\rho(\omega + i\Omega) - i\gamma\Omega) / (\omega^2 + i\omega(\Gamma + \Omega) - \Gamma\Omega - \omega_0^2), \quad (\text{A8})$$

$$\langle T_{tx} T_{tx} \rangle = - (\chi_{\pi\pi}(\omega + i\Omega)) / (\omega^2 + i\omega(\Gamma + \Omega) - \Gamma\Omega - \omega_0^2). \quad (\text{A9})$$

Which, given the definition of the heat current, leads to (7) and (5) in the main text.

Appendix B: Periodic holographic model

In the main text we mostly rely on the holographic model with periodic ionic lattice⁵⁶ and include a spontaneous translation symmetry breaking mechanism first introduced in⁷⁸. As outlined in the main text the action is

$$S = \int d^4x \sqrt{-g} \left(R - 2\Lambda - \frac{1}{2} (\partial\psi)^2 - \frac{\tau(\psi)}{4} F^2 - W(\psi) \right) - \frac{1}{2} \int \vartheta(\psi) F \wedge F. \quad (\text{B1})$$

The potentials are

$$V(\psi) \equiv 2\Lambda + W(\psi) = -6 \cosh(\psi/\sqrt{3}), \quad (\text{B2})$$

$$\tau(\psi) = \text{sech}(\sqrt{3}\psi), \quad \vartheta(\psi) = \frac{c_1}{6\sqrt{2}} \tanh(\sqrt{3}\psi),$$

Note that in these conventions the cosmological constant is $\Lambda = -3$ and the mass of the scalar is $m^2 = -2$. This setup is identical to the one we used earlier in^{39,64-66} and we refer the reader to these papers for the details of our calculation scheme. The solution to nonlinear equations of motion following from (B1) can be found in the ansatz

$$ds^2 = \frac{1}{z^2} \left(-Q_{tt} f(z) dt^2 + Q_{zz} \frac{dz^2}{f(z)} + Q_{xx} (dx + Q_{zx} dz)^2 + Q_{yy} (dy + Q_{ty} dt)^2 \right), \quad (\text{B3})$$

$$\mathcal{A} = A_t dt + A_y dy, \quad (\text{B4})$$

where $f = (1 - z)(1 + z + z^2 - \mu^2 z^3/4)$ and the temperature is related to the chemical potential as $T/\mu = (12 - \mu^2)/(16\pi\mu)$. All the ansatz functions are periodic in x and the period is set by the explicit modulation of the chemical potential

$$\mu(x) = \mu_0(1 + A \cos(kx)). \quad (\text{B5})$$

The ϑ -term drives the instability towards formation of the staggered current order, accompanied by the modulation of a pseudoscalar condensate (dual to the axion field) and charge density

$$\text{CDW} : \quad J_y \sim J_y^{(1)} \sin(px), \quad \Psi \sim \Psi^{(1)} \cos(px), \quad \rho_{\text{CDW}} \sim \rho_{\text{CDW}}^{(0)} + \rho_{\text{CDW}}^{(2)} \sin^2(px), \quad (\text{B6})$$

which are extracted as the subleading boundary coefficients of A_y, ψ and A_t bulk field profiles. The period of the charge modulation is twice smaller than the one of the staggered current. The presence of the homogeneous mode in $\rho(x)$ guarantees that the CDW produced in this way has a nonzero mean charge density, which appears as γ coefficient in the hydrodynamic equations. Note that the leading commensurate solutions are obtained with $p = 1/2k$ (1/1 commensurate CDW) and $p = 1/1k$ (2/1 commensurate CDW). In case when p is close to the spontaneous momentum of the instability these solutions acquire additional stability due to lock in^{65,66}.

1. Thermodynamics

In this appendix we discuss the holographic renormalization procedure⁷⁹ of our model, which allows us to extract the thermodynamic properties of our background solutions. The UV expansions of the various fields are

$$Q_{tt} = 1 + z^2 Q_{tt}^{(2)}(x) + z^3 Q_{tt}^{(3)}(x) + O(z^4) \quad (\text{B7})$$

$$Q_{zz} = 1 + z^2 Q_{zz}^{(2)}(x) + z^3 Q_{zz}^{(3)}(x) + O(z^4) \quad (\text{B8})$$

$$Q_{xx} = 1 + z^2 Q_{xx}^{(2)}(x) + z^3 Q_{xx}^{(3)}(x) + O(z^4) \quad (\text{B9})$$

$$Q_{yy} = 1 + z^2 Q_{yy}^{(2)}(x) + z^3 Q_{yy}^{(3)}(x) + O(z^4) \quad (\text{B10})$$

$$Q_{ty} = z^3 Q_{ty}^{(3)}(x) + O(z^4) \quad (\text{B11})$$

$$Q_{zx} = z^3 Q_{zx}^{(3)}(x) + O(z^4) \quad (\text{B12})$$

$$A_t = \mu(x) - z\rho(x) + O(z^2) \quad (\text{B13})$$

$$A_y = zJ_y(x) + O(z^2) \quad (\text{B14})$$

$$\psi = z^2\psi^{(2)}(x) + O(z^3) \quad (\text{B15})$$

From these expansions we can readily read-off the charge density $\rho(x)$ and the chemical potential $\mu(x)$. It is worth noting that the coefficients satisfy relations which correspond to the Ward identities $\langle T_\mu^\mu \rangle = 0$ and $\partial_\mu \langle T_\nu^\mu \rangle = F^{\mu\nu} \langle J_\nu \rangle$. These are

$$Q_{tt}^{(3)}(x) + Q_{xx}^{(3)}(x) + Q_{yy}^{(3)}(x) = 0 \quad (\text{B16})$$

$$\partial_x Q_{xx}^{(3)}(x) + \frac{1}{2}\mu'(x)\rho(x) = 0 \quad (\text{B17})$$

The counter terms which renormalize the action are those written in⁸⁰,

$$S_{\text{ren}} = S - \int d^3x \sqrt{-h} (K - 4 + \psi^2) \quad (\text{B18})$$

Therefore, we find that the components of the stress tensor read

$$\langle T_{tt} \rangle = 2 + \frac{\mu_0^2}{2} - 3Q_{tt}^{(3)}(x) \equiv \epsilon(x) \quad (\text{B19})$$

$$\langle T_{xx} \rangle = 1 + \frac{\mu_0^2}{4} + 3Q_{xx}^{(3)}(x) \quad (\text{B20})$$

$$\langle T_{yy} \rangle = 1 + \frac{\mu_0^2}{4} + 3Q_{yy}^{(3)}(x) \quad (\text{B21})$$

$$\langle T_{ty} \rangle = 3Q_{ty}^{(3)}(x) \quad (\text{B22})$$

The entropy density is given by the area density of the black hole as

$$s(x) = \frac{1}{4} \sqrt{Q_{xx}(x, 1)Q_{yy}(x, 1)} \quad (\text{B23})$$

Equipped with these results, we can evaluate the thermodynamic quantities of our background solutions. As shown on the middle panel of Fig. 7, the identity $\rho\mu + sT = T_{xx} + T_{yy}$ (taking the spatial average on both sides) is satisfied in the solutions which we are considering.

2. Conductivities

In order to evaluate the matrix of AC thermoelectric conductivities we consider the perturbative time dependent sources $\{\frac{\Delta_x T}{T}, E_x\}$ to the modes δg_{tx} and δA_x , correspondingly. This leads, in DeDonder gauge⁵⁸ to the excitation of the total of 15 fields, coupled at the linear order. Technically, we find it quite important to introduce the sources explicitly by expanding the fluctuation profiles near the boundary. These expansions can be obtained by solving the equations of motion order by order at $z \rightarrow 0$. In particular we use:

$$\delta A_x(z, x, t) = e^{-i\omega t} (1 - z^4)^{-\frac{i\omega}{P(1)}} \left(E_x + \tilde{A}_x(z, x) \right), \quad P(1) \equiv 3 - \frac{\mu^2}{4} \quad (B24)$$

$$\delta g_{tx}(z, x, t) = e^{-i\omega t} \frac{1}{z^2} (1 - z^4)^{-\frac{i\omega}{P(1)}} \left(\frac{\Delta_x T}{T} + \frac{1}{6} \frac{\Delta_x T}{T} z^2 \omega^2 + z^2 \tilde{g}_{tx}(z, x) \right) \quad (B25)$$

$$\delta g_{xz}(z, x, t) = e^{-i\omega t} \frac{1}{f(z) z^2} (1 - z^4)^{-\frac{i\omega}{P(1)}} \left(\frac{i}{3} \frac{\Delta_x T}{T} z \omega + \frac{i}{6} \frac{\Delta_x T}{T} z^3 \omega^3 + z^3 \tilde{g}_{xz}(z, x) \right), \quad (B26)$$

and solve the linear perturbation equations for $\{\tilde{A}_x, \tilde{g}_{tx}, \tilde{g}_{xz}, \dots\}$. These redefinitions allow us to read off the expectation values as

$$\langle J_x \rangle(x) = \partial_z \tilde{A}_x(z, x) \Big|_{z=0}, \quad \langle T_{tx} \rangle(x) = (-3) \partial_z \tilde{g}_{tx}(z, x) \Big|_{z=0}. \quad (B27)$$

In order to get rid of the contribution of the contact terms we subtract the real part of the correlator at zero frequency from the AC results⁸¹. As a nontrivial check of our calculations, we get an excellent match between $\langle J_x T_{tx} \rangle(\omega)$ and $\langle T_{tx} J_x \rangle(\omega)$ correlators, which guarantees $\alpha = \bar{\alpha}$ in (6).

As mentioned in the main text, the DC conductivities can be evaluated without solving extra numerical equations of motion. In case of DC transport one can figure out the integrals of motion which allow to solve the radial evolution of the perturbation equations analytically and the problem reduces to solving a set of linear, elliptic equations (Stoke's equations) involving horizon data of the background solutions. In the particular case of 1D holographic lattices, this can be done by a series of spatial integrations so that we can arrive at closed, yet cumbersome, expressions. For our specific model, the general 1D expressions can be found in⁶⁹. This allows us to expand our analysis to lower temperatures, where the AC methods are too demanding.

Appendix C: Fitting of AC peaks

The AC conductivities are obtained as a series of data points at various frequencies ω . We fit this data in two stages. First we expand the data symmetrically to the negative frequencies and then find the maximum of the peak at $\omega = \hat{\omega}_0$. We fit the data with a pair of symmetric Lorentzians centered at $\hat{\omega}_0$ and $-\hat{\omega}_0$ as well as a constant background. More concretely, we fit the data to

$$W_0(\omega) = C_0 + \frac{A_0}{(\omega - \hat{\omega}_0)^2 + \Sigma_0^2} + \frac{A_0}{(\omega + \hat{\omega}_0)^2 + \Sigma_0^2} \quad (C1)$$

This gives a first approximation to the position, the width and the height of the peaks $\hat{\omega}_0$, Σ_0 , and A_0 . As a second stage we fit the data with the ansatz function, which allows a leading order ω -dependence in the numerator, taking into account the asymmetry of the peaks. We use the results of the previous fit as the seed parameters. We fit the parameters to the model

$$W_1(\omega) = C_1 + \frac{A_1 - B_1(\omega^2 - \hat{\omega}_1^2)}{(\omega^2 - \hat{\omega}_1^2)^2 + \omega^2 \Sigma_1^2} \quad (C2)$$

Now take a look at the expressions for the AC conductivities of the main text. In the regime of weak pinning, we can consider Γ , Ω and ω_0 as small parameters, as compared to the thermodynamic quantities and hydrodynamic coefficients, which are finite even without pinning. The exact scalings are model dependent, but for the case of 1/2 lock-in phase, which we consider in the text, the scaling is $\Gamma \sim \lambda^2$, while $\Omega \sim \lambda$ and $\omega_0 \sim \lambda^{1/2}$ ³⁹ (where $\lambda \sim A$ is the scale of explicit symmetry breaking). We can now expand all the coefficients in front of ω , leaving only the leading

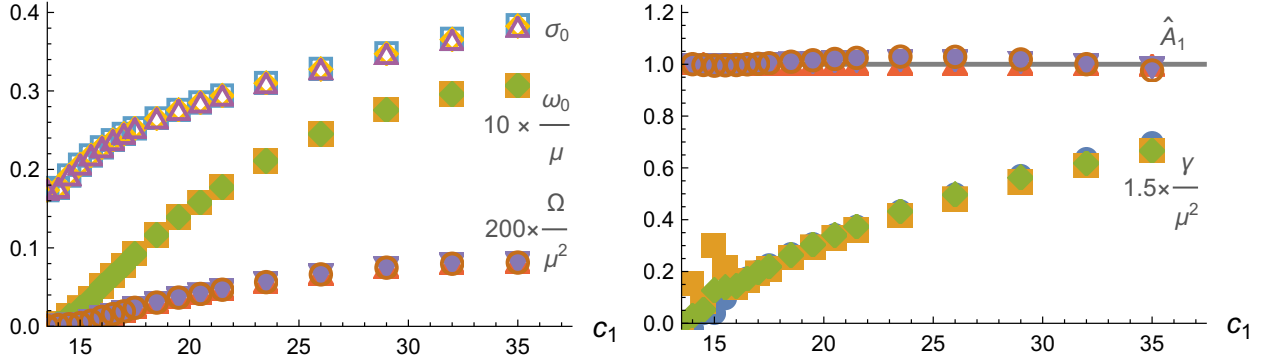


FIG. 6: The fitting parameters, as obtained from the independent fits of AC electric and thermal conductivities as well as thermopower with the function (C2). **The left panel** shows that the bare parameters match perfectly well between the fits. **The right panel** shows the agreement between the thermodynamic quantities obtained from the AC fits and evaluated on the background solutions. It also demonstrates the lesser accuracy in γ -parameter in the regime of weaker order parameter.

terms:

$$\begin{aligned} \sigma(\omega) &= \sigma_0 + \frac{(\tilde{\rho}^2\Omega - 2\tilde{\rho}\tilde{\gamma}\omega_0^2) - i\omega\tilde{\rho}^2}{\mu_0^2\chi_{\pi\pi}(-\omega^2 - i\omega\Omega + \omega_0^2)} \\ \frac{T}{\mu_0}\alpha(\omega) &= -\sigma_0 + \frac{(\tilde{\rho}\tilde{s}\Omega - (\tilde{s} - \tilde{\rho})\tilde{\gamma}\omega_0^2) - i\omega\tilde{\rho}\tilde{s}}{\mu_0^2\chi_{\pi\pi}(-\omega^2 - i\omega\Omega + \omega_0^2)} \\ \frac{T}{\mu_0^2}\bar{\kappa}(\omega) &= \sigma_0 + \frac{(\tilde{s}^2\Omega + 2\tilde{s}\tilde{\gamma}\omega_0^2) - i\omega\tilde{s}^2}{\mu_0^2\chi_{\pi\pi}(-\omega^2 - i\omega\Omega + \omega_0^2)}, \end{aligned} \quad (C3)$$

The linear frequency dependence of the numerator in these expressions leads to an asymmetric peak of the form (C2) in the real part of the conductivity. More precisely (and taking into account the definitions of tilde-parameters from the main text), the corresponding values of the fitting parameters are

$$\begin{aligned} \sigma : \quad C_1 &= \sigma_0, & A_1 &= \frac{\rho^2}{\chi_{\pi\pi}}\Omega\omega_0^2, & B_1 &= -2\frac{\rho}{\chi_{\pi\pi}}\Omega\gamma, & \Sigma_1 &= \Omega, & \hat{\omega}_1 &= \omega_0 \\ \frac{T}{\mu}\alpha : \quad C_1 &= -\sigma_0, & A_1 &= \frac{sT\rho}{\mu\chi_{\pi\pi}}\Omega\omega_0^2, & B_1 &= \frac{\mu\rho - sT}{\mu\chi_{\pi\pi}}\Omega\gamma, & \Sigma_1 &= \Omega, & \hat{\omega}_1 &= \omega_0 \\ \frac{T}{\mu^2}\kappa : \quad C_1 &= \sigma_0, & A_1 &= \frac{(sT)^2}{\mu^2\chi_{\pi\pi}}\Omega\omega_0^2, & B_1 &= 2\frac{sT}{\mu\chi_{\pi\pi}}\Omega\gamma, & \Sigma_1 &= \Omega, & \hat{\omega}_1 &= \omega_0 \end{aligned} \quad (C4)$$

We see that from each fit we can obtain σ_0 , Ω and ω_0 directly and independently. As we show on Fig. 6 (left panel), the parameters obtained this way match perfectly well with each other. As another, more nontrivial consistency check, we can extract certain thermodynamic quantities (see (C4)) from the fit of A_1 , using Ω and ω_0 and compare them with the same quantities extracted as the expectation values of the corresponding operators for the background solutions. We plot the ratio of these differently obtained thermodynamic quantities (\hat{A}_1) on the right panel of Fig. 6 and see that it matches unity within a few percent margin. Finally, the γ -coefficient is related to the B_1 – the peak asymmetry parameter, which has the highest numerical uncertainty.⁸² Nonetheless, it shows a very good agreement in the regime of larger c_1 , where the peaks are wider and the quality of fitting improves, this is shown on the right panel of Fig. 6 as well.

Another important cross check of our results is the comparison with the DC conductivities, which can be evaluated given only the near horizon data of the background solutions. We plug in the parameters obtained from the AC fits (C4) to the expressions for DC conductivities listed in the main text and compare this to the DC conductivities evaluated directly from the horizon data. As we show on Fig. 7, they agree perfectly well.

Appendix D: Helical Bianchi VII holographic model

We have checked that α also changes sign as we vary the temperature in the Bianchi VII solutions that break translations homogeneously. Our setup and notation closely follow^{39,48}. The model is defined in 5-dimensional bulk

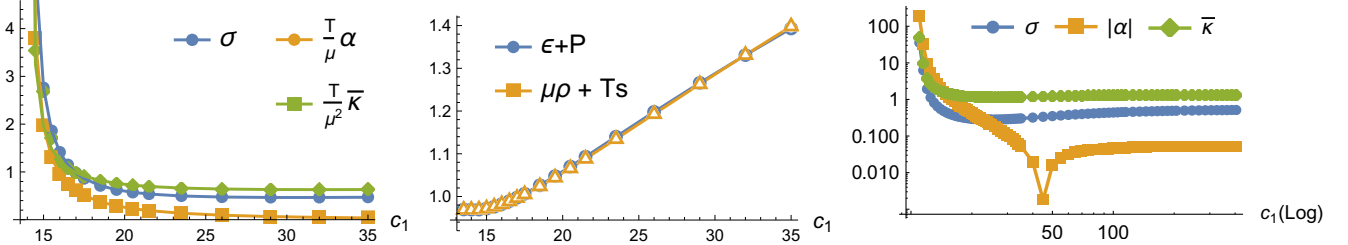


FIG. 7: **Left panel:** Comparison between the DC conductivities obtained directly from the horizon data and those evaluated with (9) using the hydrodynamic parameters extracted from AC fits. **Middle panel:** Check of the thermodynamic identity in the pseries of periodic backgrounds. **Right panel:** Evolution of DC conductivities in periodic model at large c_1 . (Log-Log scale). This continues the data shown on the left panel. The change of sign in α is evident here at strong order regime, similarly to the behavior at small tempeperatuve shown on Fig. 2.

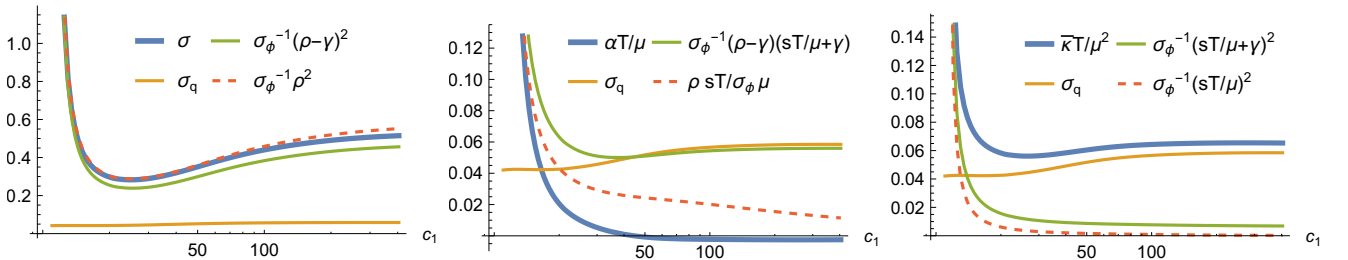


FIG. 8: The contributions to DC conductivities from various terms in (9) in a series of coupling c_1 in the periodic model. At high c_1 , the electric conductivity is dominated by the σ_ϕ^{-1} term, the heat conductivity – by σ_q -term, while the thermopower is a result of a fine balance between them. Red lines assume $\gamma = 0$ and help to appreciate the role of γ . Data as on Fig. 7 for $T/\mu = 0.1$.

($x^\mu = \{t, x, y, z, u\}$, u – radial holographic coordinate, with boundary at $u = 0$) with dynamical gravity, an Abelian gauge field A_μ , dual to the chemical potential and an auxiliary vector field B_μ , which we use to source the explicit translational symmetry breaking. The action reads

$$S = \int d^5x \sqrt{-g} \left(R - 2\Lambda - \frac{1}{4}F^2 - \frac{1}{4}W^2 \right) - \frac{\gamma CS}{6} \int A \wedge F \wedge F, \quad (D1)$$

where $\Lambda = -6$ and $F \equiv dA$, $W \equiv dB$ – the field strength tensors. As shown in^{83,84} the model in absence of explicit breaking source develops an instability at a γ_{CS} -dependent critical temperature, which leads to a formation of the structure characterized by the helical forms

$$\begin{aligned} \omega_1^{(k)} &= dx \\ \omega_2^{(k)} &= \cos(kx)dy - \sin(kx)dz \\ \omega_3^{(k)} &= \sin(kx)dy + \cos(kx)dz. \end{aligned} \quad (D2)$$

We break translations explicitly preserving the shape of the helix, by introducing the field B_μ , with boundary condition

$$B|_{u \rightarrow 0} = \lambda \omega_2^{(k)}, \quad (D3)$$

so that the conductivity matrix is finite at zero frequency^{85,86}. We take the ansatz

$$ds^2 = u^{-2}[-Tf dt^2 + U/f du^2 + W_1(\omega_1^{(k)})^2 + W_2(\omega_2^{(k)} + Qdt)^2 + W_3(\omega_3^{(k)})^2] \quad (D4)$$

$$A = A_t dt + A_2 \omega_2^{(k)} \quad (D5)$$

$$B = B_t dt + B_2 \omega_2^{(k)} \quad (D6)$$

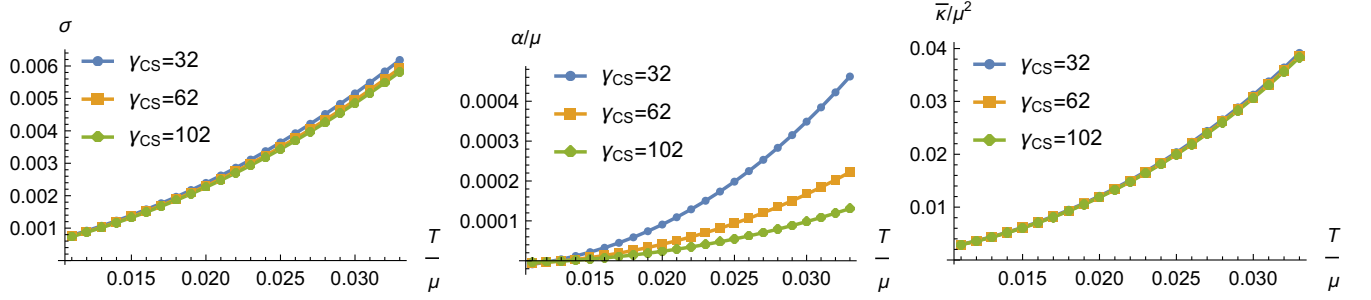


FIG. 9: The evolution DC thermo-electric conductivities at small temperatures. The holographic helical model with different values of the coupling γ_{CS} is considered. Data taken for $k/\mu = 0.76$, $\lambda/\mu = 0.3$.

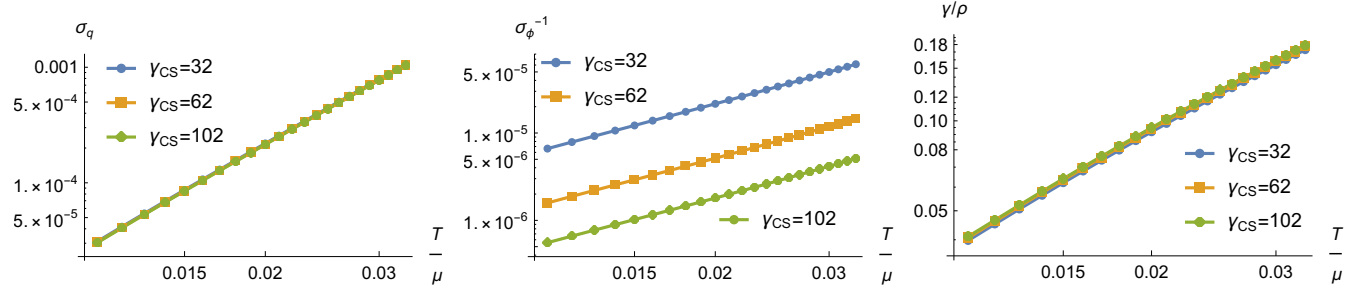


FIG. 10: Behavior of the effective theory parameters at low temperatures in the holographic helical model in Log-Log scales. The incoherent conductivity σ_q and Goldstone diffusivity behave as certain power laws, but the former does not depend on the coupling γ_{CS} . Same data as on Fig. 9.

where

$$f = (1 - u^2)(1 + u^2 - \mu^2 u^4/3) \quad (D7)$$

All unknowns are functions of the radial coordinate u only. We impose the DeTurk gauge as in⁸⁷. The normal phase is the Schwarzschild AdS solution with

$$T = U = W_i = 1, \quad Q = 0, \quad A_t = \mu(1 - u^2), \quad A_2 = B_t = B_2 = 0. \quad (D8)$$

At $\gamma_{CS} = 3$, the marginal mode of highest temperature occurs at³⁹

$$k/\mu = 2.18, \quad (T/\mu)_c = 0.223 \quad (D9)$$

Taking this as a starting point, we turn on $\lambda > 0$ and build a various families of solutions which break translations spontaneously and explicitly for increasing γ_{CS} . The DC conductivities in terms of horizon data are given in Appendix C of⁴⁸. Performing the same analysis as for the periodic model in the main text, we arrive at the results summarized on Figs. 9, 10, 11, which are in a perfect qualitative agreement with the periodic case.

Appendix E: Checks of the entropy bound

In^{27,41} it has been suggested that at low temperatures the Goldstone diffusivity is saturated by the entropy current, which leads to the universal relaxation bound $\gamma \sim \frac{\mu}{sT} \sigma_\phi \sigma_0$. This saturation has been checked in the homogeneous Q-lattice holographic model. Here we demonstrate how this bound comes about in our data. As one can see on Fig. 12, there are no signs of saturation in our examples. The possible reasons for that might be the presence of θ -term and Chern-Simons term in our models, which has not been considered in^{27,41}, or simply the fact that we don't reach low enough temperature. Otherwise, the absence of saturation here may simply point out that the above mechanism model dependent and may or may not dominate the Goldstone relaxation in different setups.

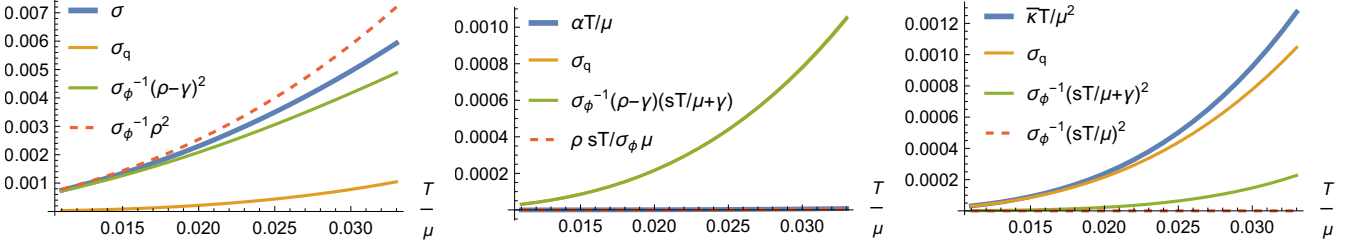


FIG. 11: Contributions to DC conductivities from various terms in (9) in the holographic helical model. At low T , the electric conductivity is dominated by σ_ϕ^{-1} term, the heat conductivity – by the σ_q -term, while thermopower is a result of a fine balance between them. This is the same behavior as for the periodic model in the main text. Red lines assume $\gamma = 0$ and help to appreciate the role of γ . Data as on Fig. 9 for $\gamma_{CS} = 62$.

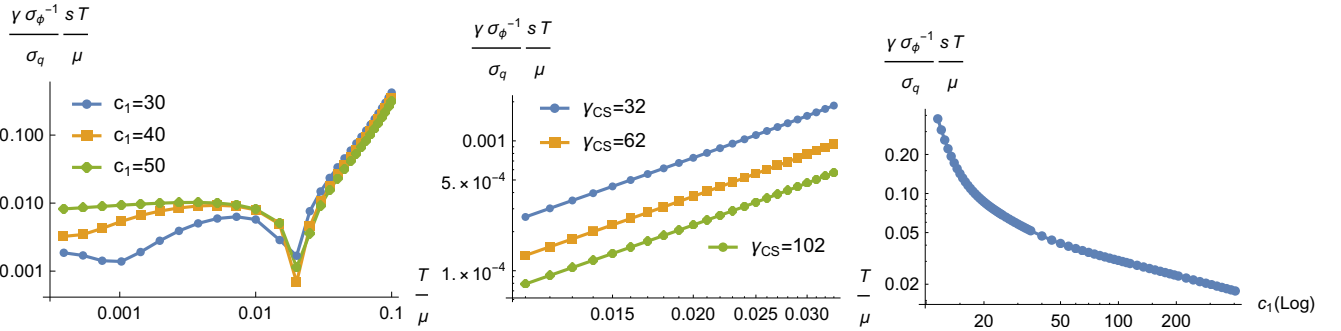


FIG. 12: Checks of the universal relaxation bound suggested in^{27,41}. **Left panel:** T series in the periodic model, data as on Fig. 2. **Middle panel:** T series in helical model, data as on Fig. 9. **Right panel:** c_1 series in the periodic model, data as on Fig. 8. We do not observe the saturation of the bound ($\gamma sT/\sigma_q \sigma_\phi \mu \approx 1$) in any of the cases.

¹ R. Arpaia and G. Ghiringhelli, Journal of the Physical Society of Japan **90**, 111005 (2021).

² C. Collignon, A. Ataei, A. Gourgout, S. Badoux, M. Lizaire, A. Legros, S. Licciardello, S. Wiedmann, J.-Q. Yan, J.-S. Zhou, *et al.*, Physical Review B **103**, 155102 (2021).

³ M. Hücker, V. Kataev, and J. Pommer, J. Phys. Chem. Solids **59**, 1821 (1998).

⁴ Y. Nakamura and S. Uchida, Physical Review B **46**, 5841 (1992).

⁵ Q. Li, M. Hücker, G. Gu, A. Tsvelik, and J. Tranquada, Physical Review Letters **99**, 067001 (2007).

⁶ J. Chang, R. Daou, C. Proust, D. LeBoeuf, N. Doiron-Leyraud, F. Laliberté, B. Pingault, B. Ramshaw, R. Liang, D. Bonn, *et al.*, Physical Review Letters **104**, 057005 (2010).

⁷ N. Doiron-Leyraud, S. Lepault, O. Cyr-Choiniere, B. Vignolle, G. Grissonnanche, F. Laliberté, J. Chang, N. Barišić, M. Chan, L. Ji, *et al.*, Physical Review X **3**, 021019 (2013).

⁸ S. Badoux, S. Afshar, B. Michon, A. Ouellet, S. Fortier, D. LeBoeuf, T. Croft, C. Lester, S. Hayden, H. Takagi, *et al.*, Physical Review X **6**, 021004 (2016).

⁹ F. Laliberté, J. Chang, N. Doiron-Leyraud, E. Hassinger, R. Daou, M. Rondeau, B. Ramshaw, R. Liang, D. Bonn, W. Hardy, *et al.*, Nature Communications **2**, 1 (2011).

¹⁰ B. Keimer, S. A. Kivelson, M. R. Norman, S. Uchida, and J. Zaanen, Nature **518**, 179 (2015).

¹¹ T. J. Reber, X. Zhou, N. Plumb, S. Parham, J. Waugh, Y. Cao, Z. Sun, H. Li, Q. Wang, J. Wen, *et al.*, Nature communications **10**, 1 (2019).

¹² J. Ayres, M. Berben, M. Čulo, Y.-T. Hsu, E. van Heumen, Y. Huang, J. Zaanen, T. Kondo, T. Takeuchi, J. Cooper, *et al.*, Nature **595**, 661 (2021).

¹³ A. Gourgout, G. Grissonnanche, F. Laliberté, A. Ataei, L. Chen, S. Verret, J.-S. Zhou, J. Mravlje, A. Georges, N. Doiron-Leyraud, *et al.*, arXiv preprint arXiv:2106.05959 (2021).

¹⁴ A. Georges and J. Mravlje, arXiv preprint arXiv:2102.13224 (2021).

¹⁵ P. Chaikin and T. Lubensky, *Principles of Condensed Matter Physics* (Cambridge University Press, 2000).

¹⁶ P. Kovtun, J. Phys. A **45**, 473001 (2012), arXiv:1205.5040 [hep-th].

¹⁷ L. D. Landau and E. M. Lifshitz, *Course of theoretical physics* (Elsevier, 2013).

¹⁸ D. T. Son, Int. J. Mod. Phys. A **16S1C**, 1284 (2001), arXiv:hep-ph/0011246.

¹⁹ L. V. Delacrétaz, B. Goutéraux, and V. Ziogas, (2021), arXiv:2111.13459 [hep-th].

²⁰ J. Armas, A. Jain, and R. Lier, (2021), arXiv:2112.14373 [hep-th].

²¹ L. V. Delacrétaz, B. Goutéraux, S. A. Hartnoll,

and A. Karlsson, Phys. Rev. **B96**, 195128 (2017), arXiv:1702.05104 [cond-mat.str-el].

²² L. V. Delacrétaz, B. Goutéraux, S. A. Hartnoll, and A. Karlsson, SciPost Phys. **3**, 025 (2017), arXiv:1612.04381 [cond-mat.str-el].

²³ G. Grüner, Rev. Mod. Phys. **60**, 1129 (1988).

²⁴ J. Zaanen, Y.-W. Sun, Y. Liu, and K. Schalm, *Holographic Duality in Condensed Matter Physics* (Cambridge Univ. Press, 2015).

²⁵ S. A. Hartnoll, A. Lucas, and S. Sachdev, (2016), arXiv:1612.07324 [hep-th].

²⁶ B. Goutéraux, N. Jokela, and A. Pönni, JHEP **07**, 004 (2018), arXiv:1803.03089 [hep-th].

²⁷ A. Amoretti, D. Areán, B. Goutéraux, and D. Musso, JHEP **10**, 068 (2019), arXiv:1904.11445 [hep-th].

²⁸ A. Amoretti, D. Areán, B. Goutéraux, and D. Musso, Phys. Rev. D **97**, 086017 (2018), arXiv:1711.06610 [hep-th].

²⁹ M. Baggioli and B. Goutéraux, (2022), arXiv:2203.03298 [hep-th].

³⁰ J. Armas and A. Jain, JHEP **01**, 126 (2020), arXiv:1908.01175 [hep-th].

³¹ J. Armas and A. Jain, Phys. Rev. D **101**, 121901 (2020), arXiv:2001.07357 [hep-th].

³² R. Arpaia, E. Andersson, E. Trabaldo, T. Bauch, and F. Lombardi, Phys. Rev. Materials **2**, 024804 (2018).

³³ H. Takagi, B. Batlogg, H. Kao, J. Kwo, R. J. Cava, J. Krajewski, and W. Peck Jr, Physical review letters **69**, 2975 (1992).

³⁴ F. Laliberté, W. Tabis, S. Badoux, B. Vignolle, D. Destraz, N. Momono, T. Kurosawa, K. Yamada, H. Takagi, N. Doiron-Leyraud, *et al.*, arXiv preprint arXiv:1606.04491 (2016).

³⁵ A. Amoretti, D. Arean, D. K. Brattan, and N. Magnoli, JHEP **05**, 027 (2021), arXiv:2101.05343 [hep-th].

³⁶ A. Amoretti, D. Arean, D. K. Brattan, and L. Martinoia, (2021), arXiv:2107.00519 [hep-th].

³⁷ Generalization to d -spatial dimensions is trivial.

³⁸ α here characterizes the “wavelength” of the CDW, however it can be chosen arbitrarily given reparametrization freedom of ϕ .

³⁹ T. Andrade, M. Baggioli, and A. Krikun, JHEP **03**, 292 (2021), arXiv:2009.05551 [hep-th].

⁴⁰ In³¹ the extra thermodynamic quantity, “lattice pressure” plays a significant role in the model. It must be zero for thermodynamically stable solutions, but can emerge in some holographic models²⁹. We mainly focus on DC conductivities, which do not depend on it, so we drop it from the equations here. The complete expressions for AC thermoelectric transport coefficients can be found in³⁶.

⁴¹ A. Amoretti, D. Areán, B. Goutéraux, and D. Musso, Phys. Rev. Lett. **123**, 211602 (2019), arXiv:1812.08118 [hep-th].

⁴² R. A. Davison and B. Goutéraux, JHEP **09**, 090 (2015), arXiv:1505.05092 [hep-th].

⁴³ R. A. Davison, B. Goutéraux, and S. A. Hartnoll, JHEP **10**, 112 (2015), arXiv:1507.07137 [hep-th].

⁴⁴ R. A. Davison, S. A. Gentle, and B. Goutéraux, Phys. Rev. Lett. **123**, 141601 (2019), arXiv:1808.05659 [hep-th].

⁴⁵ R. A. Davison, S. A. Gentle, and B. Goutéraux, Phys. Rev. D **100**, 086020 (2019), arXiv:1812.11060 [hep-th].

⁴⁶ M. Ammon, M. Baggioli, and A. Jiménez-Alba, JHEP **09**, 124 (2019), arXiv:1904.05785 [hep-th].

⁴⁷ A. Donos, D. Martin, C. Pantelidou, and V. Ziegas, Class. Quant. Grav. **37**, 045005 (2020), arXiv:1906.03132 [hep-th].

⁴⁸ T. Andrade and A. Krikun, JHEP **05**, 119 (2019), arXiv:1812.08132 [hep-th].

⁴⁹ M. Baggioli, Phys. Rev. Res. **2**, 022022 (2020), arXiv:2001.06228 [hep-th].

⁵⁰ M. Baggioli and M. Landry, (2020), arXiv:2008.05339 [hep-th].

⁵¹ C. P. Herzog, J. Phys. A **42**, 343001 (2009), arXiv:0904.1975 [hep-th].

⁵² S. A. Hartnoll, *Strings, Supergravity and Gauge Theories. Proceedings, CERN Winter School, CERN, Geneva, Switzerland, February 9-13 2009*, Class. Quant. Grav. **26**, 224002 (2009), arXiv:0903.3246 [hep-th].

⁵³ R. Flauger, E. Pajer, and S. Papanikolaou, Phys. Rev. D **83**, 064009 (2011), arXiv:1010.1775 [hep-th].

⁵⁴ Y. Liu, K. Schalm, Y.-W. Sun, and J. Zaanen, JHEP **10**, 036 (2012), arXiv:1205.5227 [hep-th].

⁵⁵ G. T. Horowitz, J. E. Santos, and D. Tong, JHEP **07**, 168 (2012), arXiv:1204.0519 [hep-th].

⁵⁶ G. T. Horowitz, J. E. Santos, and D. Tong, JHEP **11**, 102 (2012), arXiv:1209.1098 [hep-th].

⁵⁷ A. Donos and J. P. Gauntlett, JHEP **01**, 035 (2015), arXiv:1409.6875 [hep-th].

⁵⁸ M. Rangamani, M. Rozali, and D. Smyth, JHEP **07**, 024 (2015), arXiv:1505.05171 [hep-th].

⁵⁹ B. W. Langley, G. Vanacore, and P. W. Phillips, JHEP **10**, 163 (2015), arXiv:1506.06769 [cond-mat.str-el].

⁶⁰ This unidirectional crystal model allows us to simplify the treatment preserving all the necessary physics.

⁶¹ A. Donos, JHEP **05**, 059 (2013), arXiv:1303.7211 [hep-th].

⁶² B. Withers, arXiv: 1304.2011 (2013), 1304.2011.

⁶³ A. Donos and J. P. Gauntlett, JHEP **10**, 038 (2013), arXiv:1306.4937 [hep-th].

⁶⁴ A. Krikun, JHEP **12**, 030 (2018), arXiv:1710.05801 [hep-th].

⁶⁵ T. Andrade, A. Krikun, K. Schalm, and J. Zaanen, Nature Phys. **14**, 1049 (2018), arXiv:1710.05791 [hep-th].

⁶⁶ T. Andrade and A. Krikun, JHEP **03**, 168 (2017), arXiv:1701.04625 [hep-th].

⁶⁷ A vast literature is available on the holographic models which realize translation symmetry breaking in a homogeneous way^{27,29,41,46,47,88–91}, but they lack dynamical mechanism for pattern formation. We won’t discuss this approach here since we will among other things, be interested in the physics of growing order parameter. Another example of dynamical pattern formation in holography has been studied in connection to helical orders^{48,83–86,92} and we discuss it in Supplementary Material D.

⁶⁸ A. Donos, J. P. Gauntlett, T. Griffin, and V. Ziegas, JHEP **04**, 053 (2018), arXiv:1801.09084 [hep-th].

⁶⁹ A. Donos, J. P. Gauntlett, T. Griffin, N. Lohitsiri, and L. Melgar, JHEP **07**, 006 (2017), arXiv:1704.05141 [hep-th].

⁷⁰ A. Donos, J. P. Gauntlett, T. Griffin, and L. Melgar, JHEP **01**, 113 (2016), arXiv:1511.00713 [hep-th].

⁷¹ E. Banks, A. Donos, and J. P. Gauntlett, JHEP **10**, 103 (2015), arXiv:1507.00234 [hep-th].

⁷² A. Donos and J. P. Gauntlett, JHEP **11**, 081 (2014), arXiv:1406.4742 [hep-th].

⁷³ N. Iqbal and H. Liu, Phys. Rev. D **79**, 025023 (2009), arXiv:0809.3808 [hep-th].

⁷⁴ A. Romero-Bermúdez, A. Krikun, K. Schalm, and J. Zaanen, Phys. Rev. B **99**, 235149 (2019), arXiv:1812.03968

[cond-mat.str-el].

⁷⁵ F. Balm, A. Krikun, A. Romero-Bermúdez, K. Schalm, and J. Zaanen, JHEP **01**, 151 (2020), arXiv:1909.09394 [hep-th].

⁷⁶ N. Gnezdilov, A. Krikun, K. Schalm, and J. Zaanen, Phys. Rev. B **99**, 165149 (2019), arXiv:1810.10429 [cond-mat.str-el].

⁷⁷ S. Smit, E. Mauri, L. Bawden, F. Heringa, F. Gerritsen, E. van Heumen, Y. Huang, T. Kondo, T. Takeuchi, N. Hussey, *et al.*, arXiv preprint arXiv:2112.06576 (2021).

⁷⁸ A. Donos and J. P. Gauntlett, JHEP **08**, 140 (2011), arXiv:1106.2004 [hep-th].

⁷⁹ S. de Haro, S. N. Solodukhin, and K. Skenderis, Commun. Math. Phys. **217**, 595 (2001), arXiv:hep-th/0002230 [hep-th].

⁸⁰ B. Withers, Class. Quant. Grav. **30**, 155025 (2013), arXiv:1304.0129 [hep-th].

⁸¹ K.-Y. Kim, K. K. Kim, Y. Seo, and S.-J. Sin, JHEP **12**, 170 (2014), arXiv:1409.8346 [hep-th].

⁸² In the vicinity of the phase transition the analysis of the quasinormal modes, performed in³⁹ gives a better control of the physics. We are not considering this regime here.

⁸³ H. Ooguri and C.-S. Park, Phys. Rev. **D82**, 126001 (2010), arXiv:1007.3737 [hep-th].

⁸⁴ A. Donos and J. P. Gauntlett, Phys. Rev. **D86**, 064010 (2012), arXiv:1204.1734 [hep-th].

⁸⁵ A. Donos and S. A. Hartnoll, Nature Phys. **9**, 649 (2013), arXiv:1212.2998.

⁸⁶ A. Donos, B. Goutéraux, and E. Kiritsis, JHEP **09**, 038 (2014), arXiv:1406.6351 [hep-th].

⁸⁷ T. Andrade, M. Baggio, A. Krikun, and N. Poovuttikul, JHEP **02**, 085 (2018), arXiv:1708.08306 [hep-th].

⁸⁸ T. Andrade and B. Withers, JHEP **05**, 101 (2014), arXiv:1311.5157 [hep-th].

⁸⁹ A. Donos and J. P. Gauntlett, JHEP **04**, 040 (2014), arXiv:1311.3292 [hep-th].

⁹⁰ M. Baggio and O. Pujolas, Phys. Rev. Lett. **114**, 251602 (2015), arXiv:1411.1003 [hep-th].

⁹¹ L. Alberte, M. Baggio, A. Khmelnitsky, and O. Pujolas, JHEP **02**, 114 (2016), arXiv:1510.09089 [hep-th].

⁹² S. Nakamura, H. Ooguri, and C.-S. Park, Phys. Rev. D **81**, 044018 (2010), arXiv:0911.0679 [hep-th].